

Ulrike Sausbier · Matthias Sausbier · Claudia A. Sailer  
Claudia Arntz · Hans-Günther Knaus  
Winfried Neuhuber · Peter Ruth

## Ca<sup>2+</sup>-activated K<sup>+</sup> channels of the BK-type in the mouse brain

Accepted: 25 November 2005 / Published online: 14 December 2005  
© Springer-Verlag 2005

**Abstract** An antibody against the 442 carboxy-terminal amino acids of the BK channel  $\alpha$ -subunit detects high immunoreactivity within the telencephalon in cerebral cortices, olfactory bulb, basal ganglia and hippocampus, while lower levels are found in basal forebrain regions and amygdala. Within the diencephalon, high density was found in nuclei of the ventral and dorsal thalamus and the medial habenular nucleus, and low density in the hypothalamus. The fasciculus retroflexus and its termination in the mesencephalic interpeduncular nucleus are prominently stained. Other mesencephalic expression sites are periaqueductal gray and raphe nuclei. In the rhombencephalon, BK channels are enriched in the cerebellar cortex and in the locus coeruleus. Strong immunoreactivity is also contained in the vestibular nuclei, but not in cranial nerves and their intramedullary course of their roots. On the cellular level, BK channels show pre- and postsynaptic localizations, i.e., in somata, dendrites, axons and synaptic terminals.

**Keywords** BK channel distribution · Murine brain · Knock out tissue validated antibody · Immunofluorescence

Ulrike Sausbier and Matthias Sausbier have contributed equally to this work

U. Sausbier · M. Sausbier · C. Arntz · P. Ruth (✉)  
Pharmakologie und Toxikologie, Pharmazeutisches Institut  
der Universität Tübingen, Tübingen, Germany  
E-mail: peter.ruth@uni-tuebingen.de  
Tel.: +49-7071-2976781  
Fax: +49-7071-292476

C. A. Sailer · H.-G. Knaus  
Division für Molekulare und Zelluläre Pharmakologie,  
Medizinische Universität Innsbruck, Innsbruck, Austria

W. Neuhuber  
Institut für Anatomie der Friedrich-Alexander-Universität  
Erlangen-Nürnberg, Nürnberg, Germany

### Introduction

BK channels have been shown to play an important role in controlling action potential duration, firing frequency and spike frequency adaptation of many neurons by giving rise to the fast afterhyperpolarization (AHP) following a neuronal action potential (Storm 1990; Faber and Sah 2003). In the vertebrate nervous system, Ca<sup>2+</sup>-activated K<sup>+</sup> channels of the BK-type are found in axon terminals (Robitaille et al. 1999; Hu et al. 2001), somata (Levitan and Adams 1981; Storm 1987; Shao et al. 1999) and dendrites (Womack and Khodakhah 2004) of many neurons, where they activate in response to intracellular Ca<sup>2+</sup> rises through the opening of voltage-dependent (Womack et al. 2004) or neurotransmitter-gated (Isaacson and Murphy 2001) Ca<sup>2+</sup> channels, and also by Ca<sup>2+</sup> release from intracellular stores (Chavis et al. 1998) that all shift the activation voltage concentration dependently into a physiological range (Jan and Jan 1997). Lack of BK channels in pyramidal neurons such as Purkinje cells results in a less negative resting membrane potential and a decreased amplitude of the AHP, which both impairs the de-inactivation of previously inactivated voltage-dependent Na<sup>+</sup>- and Ca<sup>2+</sup> channels (Sausbier et al. 2004).

Only a single gene, KCNMA1, encodes for the pore-forming  $\alpha$ -subunit of which multiple splice variants have been described (Butler et al. 1993; Shipston 2001). The regional distribution and level of expression of the BK channel  $\alpha$ -subunit has recently been analyzed in rat brain, demonstrating that the channel is preferentially enriched in terminal areas of major projection tracts (Knaus et al. 1996). For mouse brain, however, a detailed analysis has not yet been performed, although this species has become the most commonly used mammalian resource in biomedical research. Such information is, however, crucial for the accurate interpretation of neuroscientific data obtained from genetically manipulated animals. It could not be anticipated that the BK channel expression pattern in mouse brain resembles

that from rat brain. Recent observations demonstrate differential distribution pattern of particular ion channels in the central nervous system (CNS) of both species (Hirst et al. 2003; Larm et al. 2003; Piggins et al. 2001). In an approach to study BK channel expression in the mouse, we used a specific antibody raised against a 442 amino acid comprising carboxyl terminal protein. This antibody should be able to detect all BK channel splice variants (Shipston 2001). The specificity of the antibody was proven using brain tissue from mice lacking the BK channel  $\alpha$ -subunit protein resulting from a targeted interruption of its gene. In order to accomplish a reliable semi-quantitative assessment of the BK channel distribution, we performed the immunohistological analysis on fixed [3, 3'-diaminobenzidine (DAB) method] and non-fixed [immunofluorescence (IF) method] brain tissue. The distribution observed in mouse brain implicates an important role of the BK channel in the regulation of neuronal functions.

## Materials and methods

### Mice

BK channel  $\alpha$ -subunit-deficient mice (BK<sup>-/-</sup>) were generated and maintained as described (Sausbier et al. 2004). Either litter- or age-matched wild type (wt) and BK<sup>-/-</sup> mice of both genders with hybrid SV129/C57BL6 background (always F2 generation) were used. For immunocytochemistry, the mice were always sacrificed between 12 a.m. and 1 p.m.

### BK channel $\alpha$ -subunit-specific antibody

A recombinant protein comprising of amino acid 674–1,115 of *bslo* (Accession No. 033472) with a N-terminal poly-histidine tag was generated. To obtain the fusion protein, *bslo/pcDNA3* was cut with *SmaI/BamHI* and the resulting fragment was cloned into *SmaI/PvuII* of pRSET (Invitrogen) prior to its expression in *E. coli* BL21(DE3)pLysS (Invitrogen). After induction for 3 h at 37°C with IPTG, the bacterial suspension were harvested at 10,000g for 20 min at 4°C and bacteria were resuspended in lysis buffer containing 50 mM Na<sub>3</sub>PO<sub>4</sub>, pH 8.0, 150 mM NaCl, 10  $\mu$ g/ml lysozym, 1 mM PMSF, 1 mM benzamidine-HCl, 0.2  $\mu$ g/ml leupeptin, and 1.4  $\mu$ l/ml  $\beta$ -mercaptoethanol. The suspension was subjected to a freezing–thawing cycle, homogenized using a glass–Teflon potter and centrifuged at 10,000g for 20 min at 4°C. Recombinant protein was found in inclusion bodies. Prior to their solubilization, the pellet with bacterial debris was washed stepwise with a solution containing Triton X-100 and guanidine-HCl at different concentrations in the following order [% (w/v) Triton X-100/M guanidine-HCl]: 1%/1, 1%/1.5, 2%/1.5, 2%/3, 5%/3, 0%/3 and 0%/1 M. After each step, the suspension was centrifuged at 10,000g for 20 min at

4°C and resuspended with the next step solution. Finally, inclusion bodies separated from cell debris were solubilized with buffer [50 mM Na<sub>3</sub>PO<sub>4</sub>, pH 8.0, 150 mM NaCl, 1 mM PMSF, 1 mM benzamidine-HCl, 0.2  $\mu$ g/ml leupeptin, and 1.4  $\mu$ l/ml  $\beta$ -mercaptoethanol] containing 6 M guanidine-HCl. The crude protein extract was loaded on a Ni-NTA superflow column (Qiagen), the column was washed with lysis buffer, pH 6.3, containing 6 M guanidine-HCl (10- to 30-fold of column volume) prior to elution of the fusion protein using the same buffer at pH 4.5. Subsequently, the pure fusion protein was concentrated using a Vivaspin-20 concentrator (Sartorius). The polyclonal antibody anti-BK $\alpha_{(674-1,115)}$  against the pure fusion protein was generated in rabbits. The obtained antiserum was purified at PVDF membranes (4°C overnight incubation) spotted with the recombinant fusion protein. The PVDF membranes were washed twice with 10 mM K<sub>3</sub>PO<sub>4</sub> (pH 6.8) prior to elution of the antibody with 0.1 M glycine (pH 2.5). The pH of the eluates was adjusted to pH 7.4 with 1 M K<sub>3</sub>PO<sub>4</sub> (pH 8.0), and eluates were dialyzed at 4°C overnight against storage buffer [0.5 M NaCl, 0.1 M K<sub>3</sub>PO<sub>4</sub>, 2 mM EDTA, 2 mM benzamidine-HCl; pH 7.0]. The purified antibody was concentrated using a Vivaspin-20 concentrator and stored at 4°C in storage buffer supplemented with 0.05% NaN<sub>3</sub>.

### Membrane preparations

Wt and BK<sup>-/-</sup> mice were sacrificed and their brains were quickly removed and placed in pre-chilled homogenization buffer containing 20 mM Tris, pH 8.0, 150 mM NaCl, 1 mM benzamidine-HCl, 0.2 mM PMSF, 1 mM dithiothreitol, 0.5 mM EDTA and 0.2  $\mu$ g/ml leupeptin. The brain was homogenized with an ultraturax and a glass–Teflon potter prior to centrifugation at 3,000g at 4°C for 3 min. The supernatant was collected, the pellet resuspended in homogenization buffer and centrifuged. The supernatants were pooled and ultra-centrifuged with 100,000g for 1 h at 4°C. The resulting pellet was homogenized in about 500  $\mu$ l of homogenization buffer with a glass–Teflon potter. After determination of protein concentration according to Bradford using BSA as standard, the membranes were snap-frozen and stored at –80°C.

Fifty micrograms of membrane proteins were separated by 8.5 % SDS-PAGE, blotted on a PVDF membrane and blocked with buffer (10 mM Tris, pH 8.0, 150 mM NaCl, 0.05% Tween 20) containing 5% non-fat dry milk overnight at 4°C. The PVDF membrane was washed twice for 5 min with buffer and incubated with BK $\alpha_{(674-1,115)}$  antibody (1:500 in buffer containing 5% BSA) for 1.5 h. After washing twice for 5 min with buffer containing 1% non-fat dry milk and 5 min with buffer alone, the membrane was incubated with an alkaline phosphatase-conjugated donkey anti-rabbit IgG (Dianova; 1:5,000 in buffer containing 5% BSA) for 1 h. After washing the PVDF membrane, blotted pro-

teins were visualized using the common alkaline phosphatase detection system.

### Immunohistochemistry

Wt and BK<sup>-/-</sup> mice were sacrificed and immediately perfused via the left cardiac ventricle with ice-cold PBS for 1.5 min followed by perfusion with chilled 4% paraformaldehyde in PBS for 11 min. The brains were carefully dissected, post-fixed for 1 h at 4°C, and washed for 5 min with PBS. Subsequently, the brains were incubated with an increasing sucrose gradient starting with 5% sucrose in PBS for 1 h, continuing with 10% sucrose for 8 h and finally with 20% sucrose containing 0.05% NaN<sub>3</sub> for 24 h. Thereafter, the brains were snap-frozen in isopentane (-80°C) for 2 min and then stored in air-tight vials at -80°C. Free-floating 40 μm cryostat slices (coronal sections) were performed from these brains, incubated with Tris-buffered saline (TBS) (150 mM NaCl, 100 mM Tris, pH 7.2) for 2 h, and then with TBS containing 0.5% Triton X-100 (TBS-T) for additional 2 h. The endogenous peroxidase activity was blocked with TBS containing 0.9% H<sub>2</sub>O<sub>2</sub> and 25% methanol. Tissue slices were washed for 20 min with TBS followed by two wash steps with TBS-T. After pre-incubation with buffer [1% BSA, 0.5% Triton X-100, 0.05 M TBS, pH 7.2] for 2.5 h, the brain slices were incubated overnight with anti-BK $\alpha_{(674-1,115)}$  (1:1,000 in buffer), washed for 1 h with TBS-T, and tagged with a horseradish peroxidase-conjugated goat anti-rabbit IgG (DAKO; 1:400 in buffer) for 2.5 h. Thereafter, the brain slices were rinsed 3–5 times with TBS, and the immunoreaction was visualized using the DAB method. Stained tissue sections were mounted on gelatine-coated slides, air-dried, dehydrated by an ascending ethanol series, cleared with xylene and then coverslipped with DePeX<sup>®</sup> (Serva). BK channel immunostaining was analyzed using a Leica Aristoplan microscope, fitted with appropriate filter settings and equipped with a RT color spot digital camera (Diagnostic Instruments/Visitron). In parallel, control experiments were performed using BK<sup>-/-</sup> brain slices to evaluate antibodies specificity and selectivity. The control procedures revealed no specific immunostaining in BK<sup>-/-</sup> brains.

### Immunofluorescence

Wt and BK<sup>-/-</sup> brains were carefully dissected and washed with ice-cold PO<sub>4</sub>-buffer [81 mM Na<sub>2</sub>HPO<sub>4</sub>, 19 mM NaH<sub>2</sub>PO<sub>4</sub>; pH 7.4]. Whole brains were embedded in Tissue Tek<sup>®</sup>, snap-frozen in isopentane (-40°C), and then stored at -32°C. 10 μm cryostat slices (coronal sections) were performed from wt and BK<sup>-/-</sup> brains and transferred on poly-L-lysine-coated (Sigma) slides. Brain slices were air-dried for 1 h at room temperature, rinsed for 5 min in buffer I [150 mM NaCl, 50 mM Tris; pH 7.3], and then pre-incubated for 1 h with 10% normal

goat serum (in buffer II [150 mM NaCl, 50 mM Tris, 1% BSA, 0.5% Triton X-100; pH 7.3]). After rinsing in buffer I for 5 min, the sections were incubated overnight with anti-BK $\alpha_{(674-1,115)}$  (1:1,000 in buffer II), rinsed 3×5 min in buffer I, and then incubated with an Alexa 488-conjugated goat anti-rabbit IgG (Molecular probes 1:1,000 in buffer II) for 1 h. After rinsing 3×5 min in buffer I, brain slices were coverslipped in buffer I-glycerol (1:1, pH 8.6) and stored at 4°C under light protection. BK channel immunofluorescence was analyzed using a Leica Aristoplan microscope fitted with appropriate filter settings and equipped with a RT color spot digital camera (Diagnostic Instruments/Visitron). In control experiments, the selectivity and specificity of

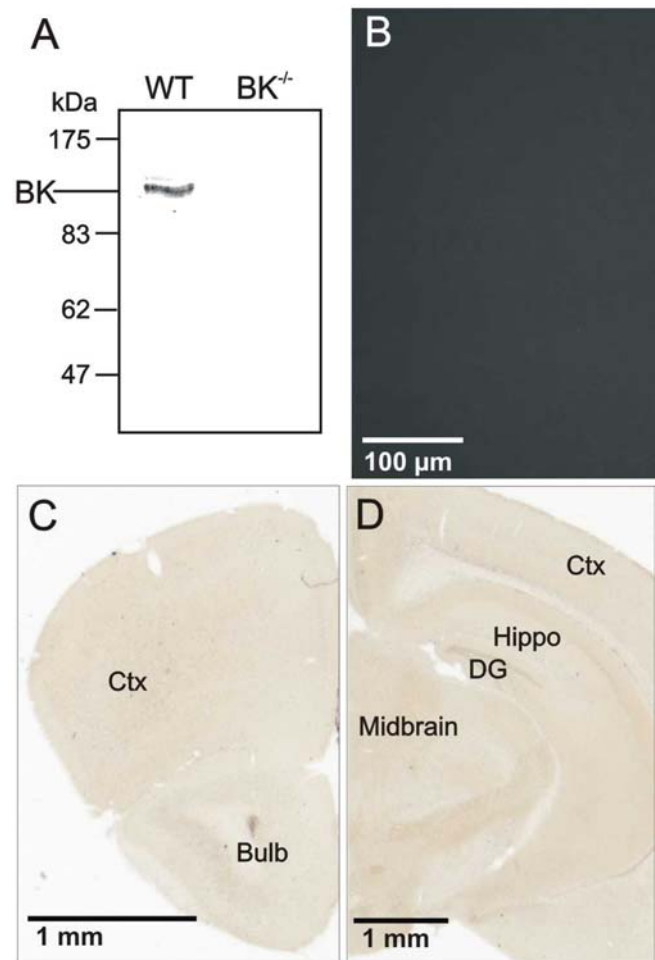


**Fig. 1** Characterization of anti-BK $\alpha_{(674-1,115)}$  antibody using Western blot analysis, immunofluorescence (IF) and immunohistochemistry (DAB method). **a** Membrane proteins (50 μg) from wt and BK<sup>-/-</sup> brains were separated by SDS-PAGE and blotted onto a PVDF membrane. **b** Anti-BK $\alpha_{(674-1,115)}$  did not show any IF in slices from BK<sup>-/-</sup> brains. The lack of IF in a representative section of stratum lucidum of the hippocampus is presented. **c** Immunostaining of BK<sup>-/-</sup> brains using the DAB method yielded only anatomical background. Representative coronal sections of olfactory bulb (*Bulb*) with cerebral cortex (*Ctx*) (**c**) and midbrain (*Midbrain*) with cerebral cortex (*Ctx*), hippocampus (*Hippo*) and dentate gyrus (*DG*) (**d**) are shown

**Table 1** Morphological structures refer to the neuro-anatomical atlas from Paxinos and Franklin (2004)

Brain region	IF	DAB
<b>Telencephalon</b>		
<i>Olfactory system</i>		
Olfactory bulb		
Glomerular layer	+ +	+ + + +
External plexiform layer	+	+ +
Mitral cell layer	±	+
Internal plexiform layer	+	+ +
Granule cell layer	+ + +	+ + +
Accessory olfactory bulb	±	±
Anterior olfactory nuclei	+ + +	+ + +
Endopiriform nuclei	+ + +	+ +
Olfactory tubercle	+ +	+ +
Islands of Calleja	+ +	+ +
Medial forebrain bundle	+ +	+ + +
Nucleus of the lateral olfactory tract	+ +	+ +
Lateral olfactory tract	-	-
<i>Cerebral cortex</i>		
Molecular layer (I)	+ + +	+ + +
External granule cell layer (II)	+ + +	+
External pyramidal cell layer (III)	+ + +	+
Internal granule cell layer (IV)	+ + +	+
Internal pyramidal cell layer (V)	+ + +	+ +
Multiform layer (VI)	+ + +	+ +
<i>Septum and basal forebrain regions</i>		
Lateral septal group		
Lateral septal nucleus	+ +	+ +
Septohippocampal nucleus	+ + +	+ +
Septofimbrial nucleus	±	-
Medial septal group		
Medial septal nucleus	±	-
Diagonal band of Broca	±	-
Posterior septal group		
Triangular septal nucleus	+ +	+
Stria medullaris	+	-
Nucleus of the anterior commissure	+	+
Ventral septal group		
Bed nuclei of the stria terminalis	+ +	+
Fusiform nucleus	+	±
Septohypothalamic nucleus	+	+
<i>Basal nuclei</i>		
Caudate putamen	+ +	+ +
Nucleus accumbens core	+ + +	+ +
Nucleus accumbens shell	+ + +	+ +
Globus pallidus	+ + +	+ + +
Ventral pallidum	+ + +	+ + +
Clastrum	+ +	+ +
Subthalamic nucleus	+	+
Entopeduncular nucleus	+ + + +	+ + + +
Substantia nigra pars reticulata	+ + + +	+ + + +
Substantia nigra pars compacta	±	±
<i>Amygdaloid complex</i>		
Extended amygdala		
Central amygdaloid nucleus	+ + +	+ +
Medial amygdaloid nucleus	+ + +	+ +
Sublentic external amygdala	+ +	+ +
Bed nucleus of the stria terminalis		
Lateral	+ +	+ +
Anterior medial	+ +	+ +
Posterior medial	+ +	+ +
Intraamygdaloid	+ +	+ +
Cortical-like nuclei		
Cortical nucleus	+ +	+ +
Lateral amygdaloid nucleus	+ +	+ +
Basolateral amygdaloid nucleus	+ +	+ +
Basomedial amygdaloid nucleus	+ +	+ +
Amygdalohippocampal area	+ +	+ +

**Table 1** (Contd.)

Brain region	IF	DAB
Amygdalopiriform transition area	+ +	+ +
Anterior amygdaloid area	+ +	+ +
Intercalated amygdaloid nuclei	+ + +	+ +
Amygdalostratial transition area	+ +	+ +
Substantia innominata	+ +	+
<i>Hippocampal formation</i>		
CA1		
Stratum oriens	+ + +	+ + +
Stratum pyramidale	±	-
Stratum radiatum	+ + +	+ +
Stratum lacunosum moleculare	+ + + +	+ +
CA2		
Stratum oriens	+ + +	+ + +
Stratum pyramidale	±	-
Stratum radiatum	+ + +	+ +
CA3		
Stratum oriens	+ + +	+ + +
Stratum pyramidale	±	-
Stratum lucidum	+ + +	+ + + +
Stratum radiatum	+ + +	+ +
Dentate gyrus		
Molecular cell layer	+ + + +	+ + +
Granule cell layer	±	-
Polymorphic layer	+ + +	+ + + +
Tenia tecta	+ +	+ +
Subiculum	+ + + +	+ + +
Parasubiculum	+ + + +	+ + +
Presubiculum	+ + + +	+ + +
Fimbria hippocampus	+	+ +
Fasciola cinereum	+ +	+ +
Indusium griseum	+ + +	+ + +
<b>Diencephalon</b>		
<i>Thalamus</i>		
Anterior thalamic nuclei	+ + +	+ + +
Midline thalamic nuclei		
Paratenial nucleus	+ +	+
Paraventricular thalamic nucleus	+ +	+ +
Reuniens thalamic nucleus	+ + +	+ + +
Rhomboid nucleus	+ +	+
Interanterior thalamic nuclei	+ +	+ +
Mediodorsal thalamic nucleus	+ + +	+ + +
Laterodorsal thalamic nucleus	+ + +	+ + +
Intermediodorsal thalamic nucleus	+ + +	+ + +
Lateral posterior thalamic nucleus	+ +	+ +
Intralaminar thalamic nuclei		
Central thalamic nuclei	+ +	+ + +
Paracentral thalamic nucleus	+ +	+ +
Parafascicular thalamic nucleus	+ +	+
Subparafascicular thalamic nucleus	+	±
Ventral thalamic nuclei	+ + +	+ + +
Posterior thalamic complex		
Limitans nucleus	+ +	+
Posterior nucleus	+ +	+
Supragenulate Nucleus	+	+
Submedial nucleus	+ +	+
Reticular thalamic nucleus	+ + +	+ + +
Lateral geniculate nucleus	+ + +	+ + +
Intergeniculate leaflet	+	±
Subgeniculate nucleus	+	±
Medial geniculate nucleus	+ +	+ + +
Xiphoid thalamic nucleus	+ +	±
Ethmoid thalamic nucleus	+ +	+
Retroethmoid thalamic nucleus	+ +	+
Prerubral field	+	+
Pretectal nuclei	+	+
Zona incerta	+	-
Medial habenular nucleus	+ + +	+ + +

Table 1 (Contd.)

Brain region	IF	DAB
Lateral habenular nucleus	±	±
Fasciculus retroflexus	+ + + +	+ + + +
<i>Hypothalamus</i>		
Hypothalamic areas	+	+
Anterior hypothalamic nucleus	+	+
Ventromedial hypothalamic nucleus	+	+
Dorsomedial hypothalamic nucleus	+	+
Preoptic area	+	+
Preoptic nuclei	+	+
Parastriatal nucleus	+	±
Periventricular nucleus	+	+
Paraventricular nucleus	+	+
Tuberal nucleus	+	+
Terete hypothalamic nucleus	+	+
Tuber cinereum area	+	+
Arcuate nucleus	+	+
Median eminence	±	±
Suprachiasmatic nucleus	+	+
Supraoptic nucleus	+	+
Nucleus of the optic tract	±	±
Nucleus supraoptic retrochiasmaticus	+	+
Retrochiasmatic hypothalamic area	+	+
Optic tract	—	—
Supraoptic decussation	—	—
Mammillary nuclei	+	+
Supramammillary nucleus	+	+
Supramammillary decussation	—	—
Mammillotegmental tract	—	—
Fornix	—	—
<i>Mesencephalon</i>		
<i>Midbrain</i>		
Superior colliculus		
Zonula layer	+	±
Superficial gray layer	+	±
Optic nerve layer	—	—
Intermediate gray layer	+	±
Intermediate white layer	+	±
Deep gray layer	+	±
Deep white layer	+	±
Deep mesencephalic nucleus	+	+
Periaqueducal gray	+ +	+ +
Nucleus of Darkewitsch	+	+
Edinger–Westphal nucleus	+ +	+ +
Medial accessory oculomotor nucleus	+	+
Supraoculomotor nucleus	+	+
Oculomotor nucleus	+	+
Interoculomotor nucleus	+	+
Interstitial nucleus of Cajal	+	+
Trochlear nucleus	+	+
Paratrochlear nucleus	+	+
Cuneiform nucleus	+	+
Red nucleus	+	+
Retrorubral field	+	+
Rape nuclei		
Dorsal raphe nucleus	+	+
Median raphe nucleus	+ +	+
Paramedian raphe nucleus	+ +	+
Rostral linear raphe nucleus	+	+
Caudal linear raphe nucleus	+ +	+
Central superior raphe nuclei	+	+
Paranigral nucleus	+	+
Ventral tegmental area	+	+
Interfascicular nucleus	+	+
Interpeduncular nucleus	+ + + +	+ + + +
Inferior colliculus		
Nucleus brachium	+	±
External cortex	+ +	+

Table 1 (Contd.)

Brain region	IF	DAB
Dorsal cortex	+ + +	+
Central cortex	+ +	+
Parabigeminal nucleus	+	+
Peripeduncular nucleus	+	+
Central gray	+ +	+
<i>Rhombencephalon</i>		
<i>Cerebellum</i>		
Cortex		
Molecular layer	+ + + +	+ + + +
Purkinje cell layer	+ + + +	+ + + +
Granule cell layer	+	+
White matter	+	+
Deep nuclei		
Nucleus interpositus	+ + + +	+ + + +
Fastigial nucleus	+ + + +	+ + + +
Dentate nucleus	+ + + +	+ + + +
<i>Pons and medulla oblongata</i>		
Pontine nuclei	+	+
Pontine gray matter	+	+
Pyramidal tract (py)	—	—
Inferior olivary complex	+	+
Superior olivary complex		
Lateral superior olive	+	+
Medial superior olive	+	+
Nucleus of the trapezoid body	+	+
Trapezoid body	—	—
Superior paraolivary nucleus	+	+
Paraolivary nuclei	+ +	+
Periolivary nuclei	+	+
Nuclei of the lateral lemniscus	+	±
Lateral lemniscus	—	—
Medial lemniscus	—	—
Principal sensory trigeminal nucleus	+ +	+
Ventrolateral tegmental area	+	+
Tegmental nuclei	+	+
Barrington nucleus	+ +	+
Sphenoid nucleus	+ +	+
Subbrachial nucleus	+	+
Parabrachial nucleus	+ +	+
Locus coeruleus	+ + +	+ +
Vestibular nuclei		
Vestibulocerebellar nucleus	+ + +	+ + +
Superior vestibular nucleus	+ + +	+ + +
Medial vestibular nucleus	+ + +	+ + +
Lateral vestibular nucleus	+ +	+ +
Spinal vestibular nucleus	+ +	+ +
Cochlear nuclei		
Anterior ventral cochlear nucleus	+	+
Posterior ventral cochlear nucleus	+	+
Dorsal cochlear nucleus	+	+
Prepositus hypoglossal nucleus	+ +	+ +
Nucleus of the solitary tract	+ +	+
Dorsal motor nucleus of the vagus	+ +	+
Spinal trigeminal nucleus	+ +	+
Nucleus X	+	+
Nucleus Y	+	+
Reticular nuclei		
Tegmental reticular nucleus	+ +	+
Gigantocellular reticular nucleus	+ +	+
Paragigantocellular reticular nucleus	+ +	+
Intermediate reticular nucleus	+	+
Parvicellular reticular nucleus	+	+
Magnocellular reticular nucleus	+	+
Rostroventrolateral reticular nucleus	+ +	+
Inferior salivatory nucleus	+	±
Rape nuclei		
Nucleus raphe magnus	+ +	+

**Table 1** (Contd.)

Brain region	IF	DAB
Nucleus raphe pallidus	+ +	+
Raphe nucleus obscurus	+ +	±
Ambiguus nucleus	+ +	+
Facial nucleus	+ +	+
Accessory facial nucleus	+ +	+
Nucleus of Roller	+	+
Intercalated nucleus medulla	+	+
Hypoglossal nucleus	+ +	+
Cuneate nucleus	+	+
External cuneate nucleus	+	+
Linear nucleus of medulla	+	+
Area postrema	+	+
Gracile nucleus	+	+
Paratrigeminal nucleus	+	+
Abducens nucleus	+	+

The intensity of BK channel immunoreactivity was classified as follows: -, negative; ±, faint; +, few; + +, moderate, intermediate; + + +, high; + + + +, very high. For evaluation, we used internal standards: for immunofluorescence evaluation, we used interpeduncular nucleus and molecular layer of dentate gyrus (+ + + +), neocortex (+ + +), intralaminar thalamic nuclei and anterior amygdaloid area (+ +), anterior hypothalamic area and pontine gray matter (+). For DAB evaluation, we used entopeduncular nucleus and polymorph layer of dentate gyrus (+ + + +), reticular thalamic nucleus (+ + +), caudate-putamen and amygdala (+ +), mammillary nuclei (+). In general, examination was performed at a magnification of 12.8×. A faint staining (±) was only observed when using a 20× magnification. Staining intensity of BK<sup>-/-</sup> slices was negative (-)

anti-BK $\alpha_{(674-1,115)}$  and the secondary antibody were tested revealing the lack of non-specific immunostaining.

## Results

### Characterization of the anti-BK $\alpha_{(674-1,115)}$ antibody

The affinity-purified antibody raised against the recombinant 442 amino acids of the carboxy-terminal domain of the BK channel specifically detects the channel in wt mouse brain membrane preparations (Fig. 1a). This antibody was subsequently used to reveal the regional expression of BK channels in mouse brain with DAB and IF methods. In contrast to specific staining observed in wt mice, no staining was found in brain sections from BK<sup>-/-</sup> mice (Fig. 1b-d). To avoid possible signal reduction or loss through masking of the antigen by paraformaldehyde or Zamboni fixation, the IF was carried out on sections of unfixed brains, whereas the common DAB method was applied to fixed tissue. However, both the methods yielded similar results when BK channel immunoreactivity was semi-quantified in a rank order reaching from negative to very high (Table 1).

### Olfactory system

The main olfactory bulb displays BK immunoreactivity at moderate levels (Fig. 2). Moderate to high channel

density is observed in the glomerular layer, where incoming sensory axons synapse on the dendrites of olfactory bulb neurons (Fig. 2a, b). Lower but still significant expression is present in the overlaying outer and internal plexiform layer (Fig. 2a, b) and the granule cell layer (Fig. 2a-c) in the depth of the olfactory bulb, while very low expression is found in the layer containing the cell bodies of the mitral cells (Fig. 2a, b), the principal relay neurons in the olfactory bulb. In turn, pronounced levels of BK channel expression is detected in the olfactory tubercles (medial forebrain bundle, mfb) (Fig. 3a) and the islands of Calleja (Table 1), tightly packed populations of granule cells adjacent to the ventral surface of the tubercle.

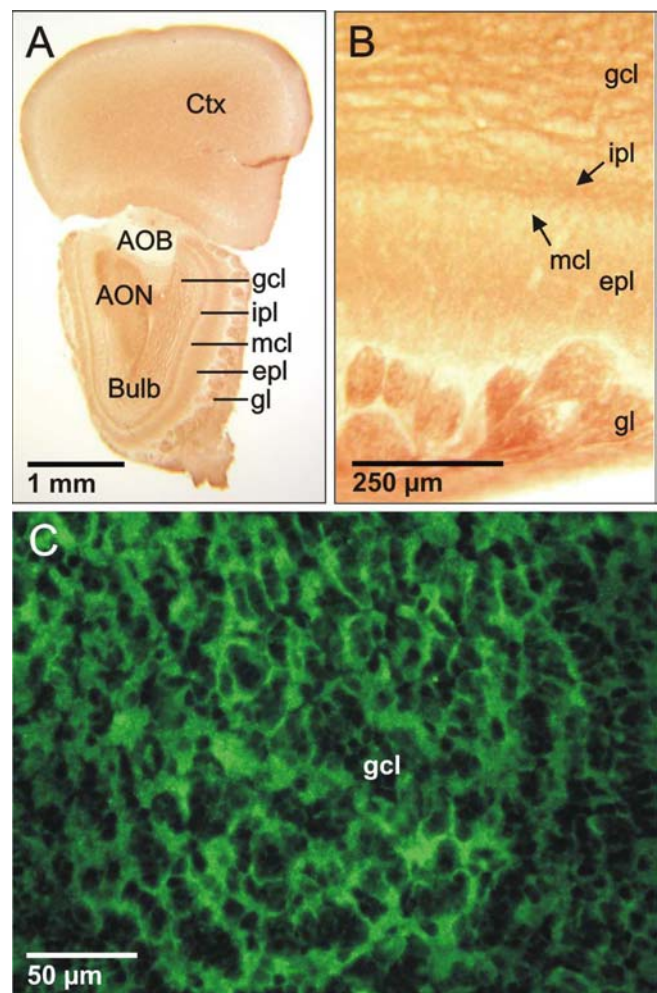


**Fig. 2** Expression sites of BK channels in the olfactory bulb (*Bulb*). **a** DAB stain revealed prominent expression in the glomerular layer (*gl*), granule cell layer (*gcl*) and the anterior olfactory nuclei (*AON*). In comparison, the external (*epl*) and internal (*ipl*) plexiform layer, and the mitral cell layer (*mcl*) displayed weaker but still pronounced immunoreactivity. In contrast, accessory olfactory bulb (*AOB*) exhibited no BK channel immunoreactivity. **b** Details of DAB stain in the olfactory bulb. **c** IF of the granule cell layer (*gcl*)

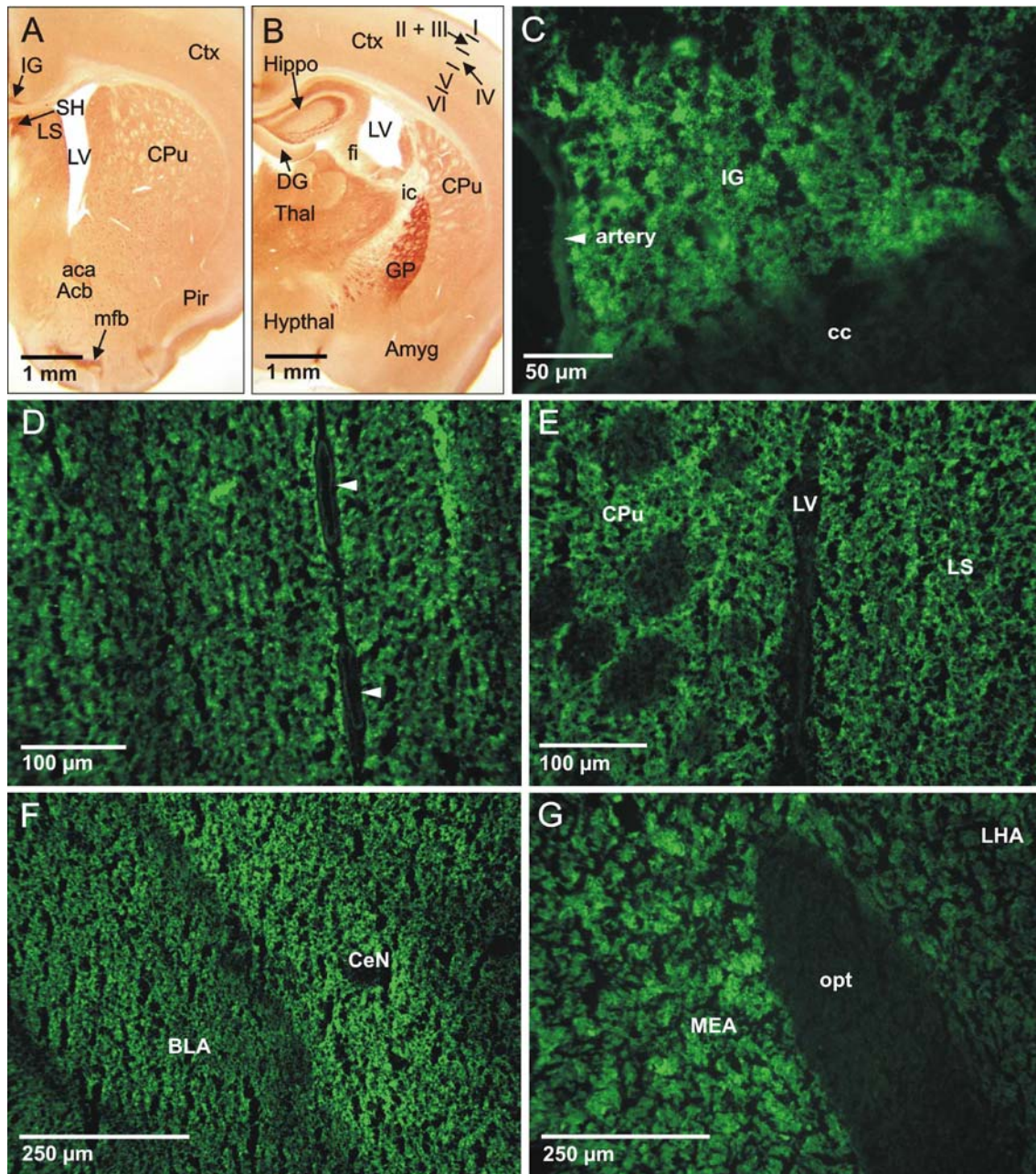


**Fig. 3** BK channel expression in telencephalic neocortex, septal regions and amygdala. **a** Overview of septal regions, neocortex (*Ctx*) and piriform cortex (*Pir*) showing intense DAB stain in the septohippocampal nucleus (*SH*) and moderate stain in the lateral septal nucleus (*LS*), both belonging to the lateral septal nucleus group. High expression sites are indusium griseum (*IG*) and medial forebrain bundle (*mfb*). Intermediate expression is found in caudate-putamen (*CPu*), nucleus accumbens (*Acb*), anterior commissure (*aca*), a bundle of nerve fibers partially connecting the olfactory bulb and the amygdala. **b** Overview of cerebral cortical (*Ctx*) layers I–VI and amygdala (*Amyg*). Note moderate to high DAB stain in hippocampus (*Hippo*), dentate gyrus (*DG*) and thalamus (*Thal*). An intense staining is visible in the globus pallidus (*GP*). The hypothalamus (*Hypthal*) and the hippocampal fimbria

(*fi*) exhibit moderate to low, the internal capsule (*ic*) very low expression. **c** IF of indusium griseum (*IG*) and corpus callosum (*cc*). The corpus callosum (*cc*) shows no immunoreactivity for BK channels. **d** Detail of neocortical BK channel distribution in retrosplenial cortex. Small brain arteries (*arrowheads*) are only faintly stained. **e** BK channel immunofluorescence in the caudate-putamen (*CPu*) and the lateral septal nucleus (*LS*) separated by the lateral ventricle (*LV*). **f** Moderate to high IF was detected throughout the cortical-like nuclei such as the basolateral amygdaloid nucleus (*BLA*) and the central amygdaloid nucleus (*CeN*). **g** IF intensities ranged between high in the medial amygdaloid nucleus (*MEA*), to low in the lateral hypothalamic area (*LHA*). The optic tract (*opt*) was not stained

## Cerebral cortex

Both, isocortex (e.g., orbital, somatosensory, auditory, visual and motor cortex) and allocortex (e.g., retrosplenial and piriform cortex) display moderate to high

BK channel expression in cortical layers I–VI. (Fig. 3b and Table 1). The neocortical distribution correlates well with *in situ* hybridization data, which reveal high BK channel mRNA levels in the different layers of the neocortex (Sausbier et al. 2004).

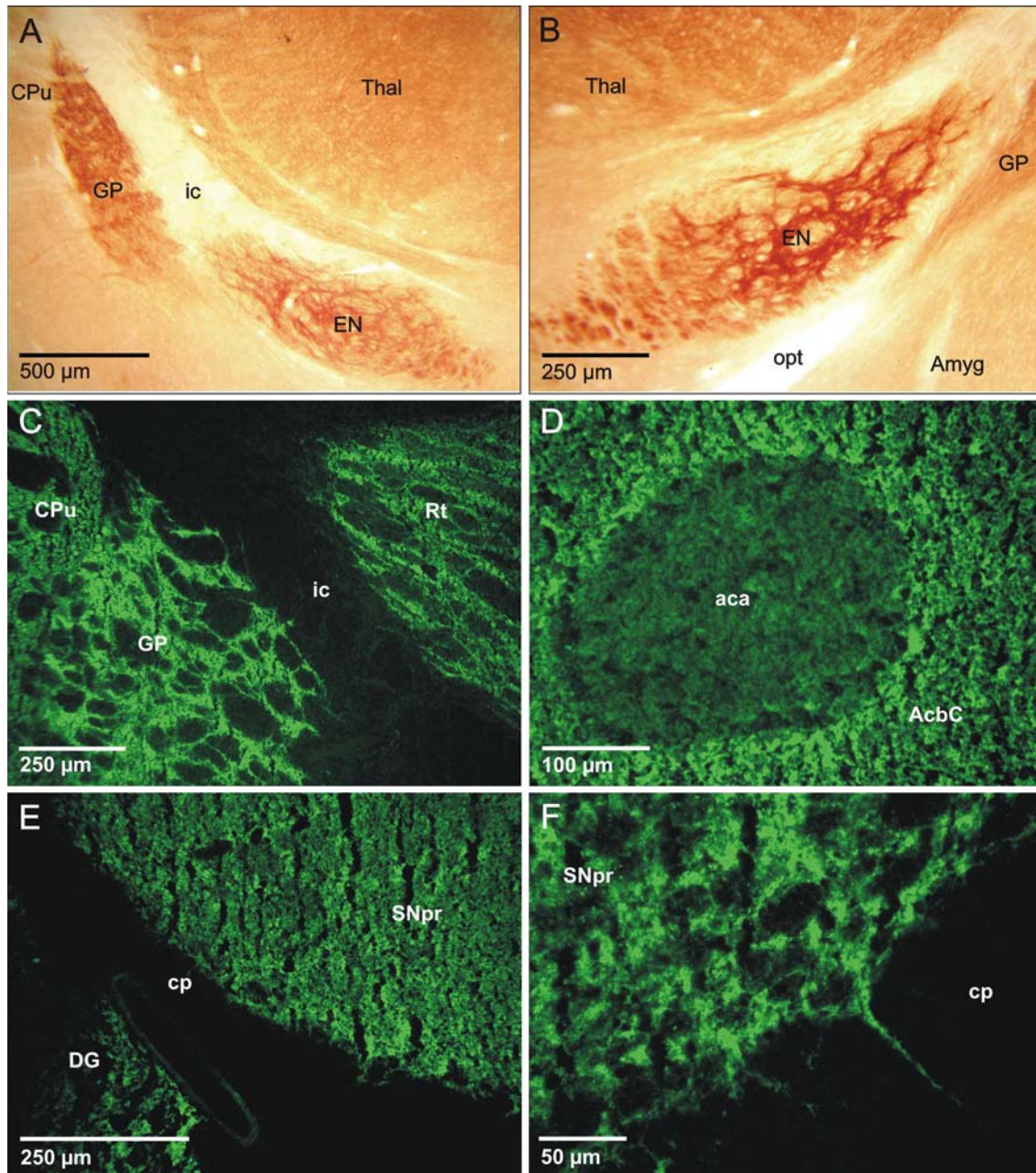


**Fig. 4** BK channel expression in basal ganglia. **a, b** DAB stain shows moderate expression in caudate-putamen (*CPu*), a very high expression in globus pallidus (*GP*) and in entopeduncular nucleus (*EN*). As in Fig. 3g, the optic tract (*opt*) is devoid of BK channels, whereas thalamus (*Thal*) and amygdala (*Amyg*) show high and moderate staining, respectively. **c** The reticular thalamic nucleus (*Rt*) which is separated from the globus pallidus (*GP*) by the internal capsule (*ic*) displays high IF. Different staining intensities confine *CPu* from *GP*. **d** Core region of the nucleus accumbens

(*AcbC*) with anterior commissure (*aca*) shows high and low to moderate IF, respectively. **e** Substantia nigra pars reticulata (*SNpr*) with very high IF, cerebral peduncle (*cp*) without IF, a small brain artery with faint IF and dentate gyrus (*DG*) with high IF. **f** IF in structures crossing the cerebral peduncle (*cp*). These structures could be axons crossing the cerebral peduncle (*cp*) and projecting to/from substantia nigra pars reticulata (*SNpr*) or neuropil of the *SNpr*, which shift into between fiber bundles of the cerebral peduncle



## Septum and amygdaloid complex

In the septal complex, most of the BK channels are present in the lateral septum (Fig. 3a, e). The medial septum with the diagonal band of Broca were devoid of BK channel immunoreactivity, whereas the posterior septum showed low expression (Table 1). The amygdaloid complex, a group of nuclei with extensive intranuclear and internuclear connections, display moderate BK channel immunostaining (Fig. 3b, f, g), similar as the amygdalostriatal transition area (Table 1).

## Basal nuclei

The striatum, the globus pallidus, the substantia nigra and the subthalamic nucleus are the four subcortical nuclei with major projections from the cerebral cortex, thalamus and certain brain stem nuclei. Within these

structures BK channels are highly concentrated in the globus pallidus (Fig. 4a, c) and the substantia nigra pars reticulata (Fig. 4e, f). Staining is most prominent in the entopeduncular nucleus (Fig. 4a, b), a major outflow nucleus of the basal ganglia projecting to several thalamic nuclei. Intermediate to high expression has been found in caudate putamen (Fig. 4a, c). The BK channel is not relevantly expressed in substantia nigra pars compacta and the subthalamic nucleus (Table 1). The nucleus accumbens which is situated adjacent to the medial and ventral parts of the caudate putamen shows intermediate stain in the core and shell region (Fig. 4d).

## Hippocampal formation

The BK channels are widely expressed in the hippocampal formation composed of hippocampus proper

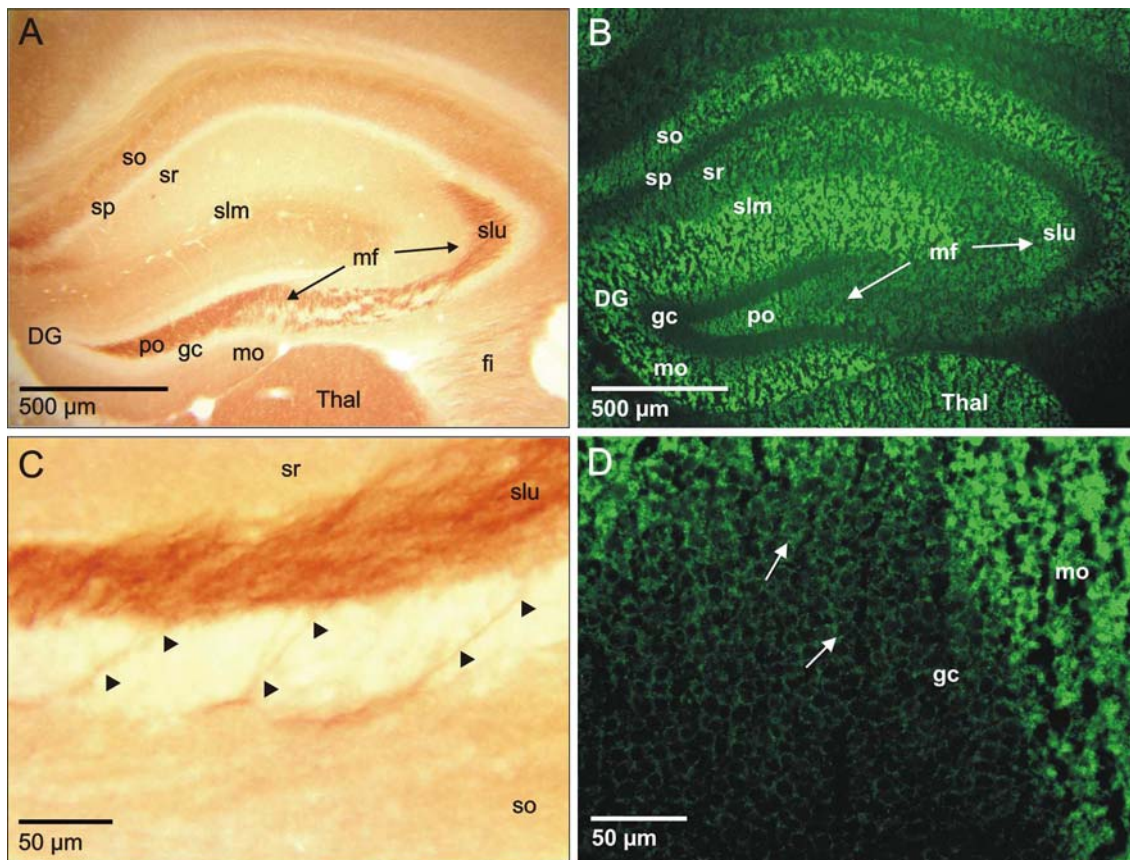


**Fig. 5** Distribution of BK channels in the hippocampal formation. Strong DAB stain (**a, c**) and IF (**b, d**) was observed in hippocampal stratum oriens (*so*) and stratum lucidum (*slu*). The stratum radiatum (*sr*) and the stratum lacunosum moleculare (*slm*) displayed moderate stain. No staining was found in the stratum pyramidale (*sp*). In the dentate gyrus (*DG*), very high immunoreactivity was obtained in the polymorph layer (*po*) and the mossy fibers (*mf*). Less but still significant immunoreactivity was contained in molecular layer (*mo*) and hippocampal fimbria (*fi*). Mostly, IF and DAB stain revealed similar intensities (**a, b**). Exceptions are the very high IF compared to a moderate DAB stain in the stratum lacunosum moleculare (*slm*), and the moderate IF compared to a

very high DAB stain in stratum lucidum (*slu*) and polymorph layer (*po*) of dentate gyrus (*DG*). As a possible explanation we suggest (1) different antibody accessibility due to fixation (DAB) and non-fixation (IF) conditions, and/or (2) increased proteolysis sensitivity under non-fixation condition that may reduce the IF signal in stratum lucidum (*slu*), mossy fibers (*mf*) and polymorph layer (*po*). **c** BK channel-expressing mossy fibers (*arrowheads*) project from the polymorph layer of dentate gyrus to the stratum lucidum (*slu*) via the stratum pyramidale. **d** Punctuated stain (*arrows*) in the granule cell layer (*gc*) presumably represents single or clustered BK channels

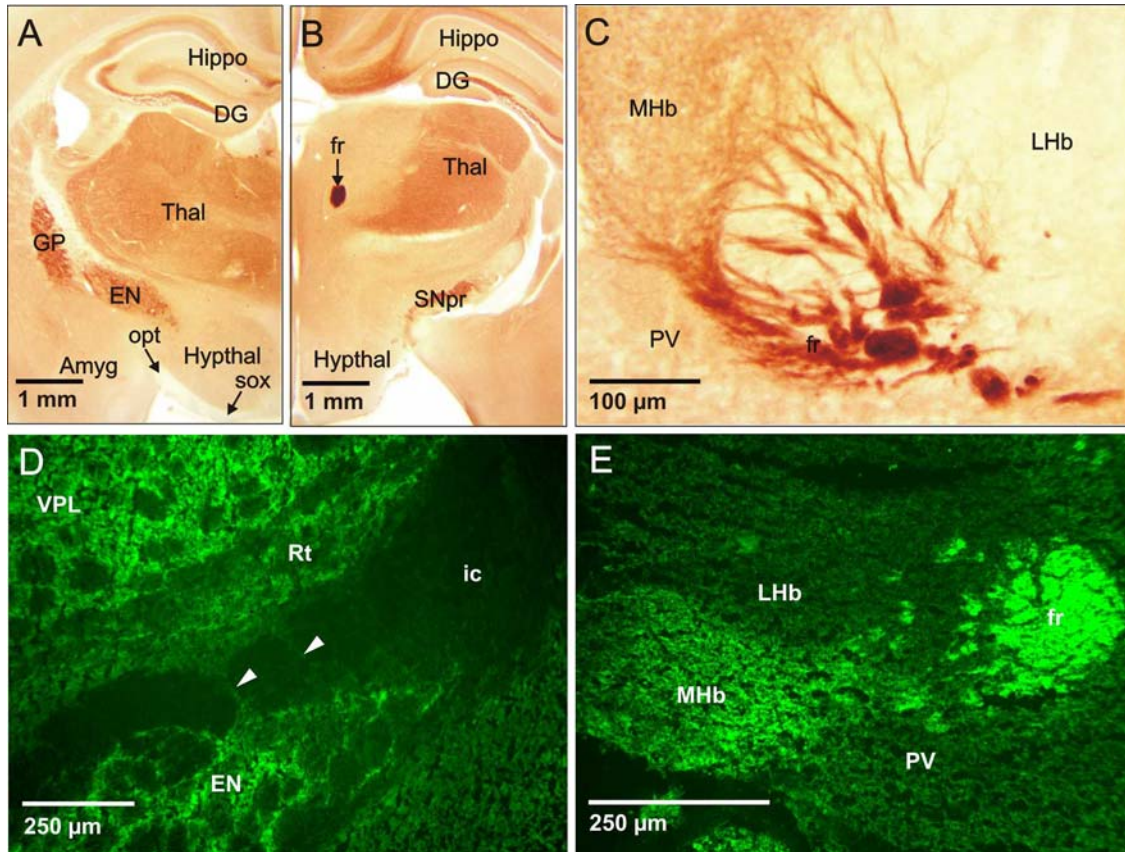


**Fig. 6** BK channel expression in the diencephalon. **a, b** The thalamic nuclei (*Thal*) exhibit moderate to high, the hypothalamus (*Hypthal*) low but still significant DAB staining. The hippocampus (*Hippo*) and dentate gyrus (*DG*) show moderate to high stain, globus pallidus (*GP*), entopeduncular nucleus (*EN*) and substantia nigra pars reticulata (*SNpr*) even very high stain. The optic tract (*opt*) and the supraoptic decussation (*sox*) are not stained. **c, e** The fasciculus retroflexus (*fr*) exhibits the highest BK channel density in the mouse brain, as revealed by DAB stain (**c**) and IF (**e**). This fiber

bundle comprises projections from the medial habenular nucleus (*MHb*). The paraventricular thalamic nucleus (*PV*) shows a moderate and the lateral habenular nucleus (*LHb*) a faint expression. **d** The thalamic nuclei such as the ventral posterior thalamic nucleus (*VPL*) and the reticular thalamic nucleus (*Rt*) display moderate to high expression. Reticular thalamic nucleus (*Rt*) and entopeduncular nucleus (*EN*) communicate by BK channel positive axons/dendrites (*arrowheads*) via the internal capsule (*ic*)

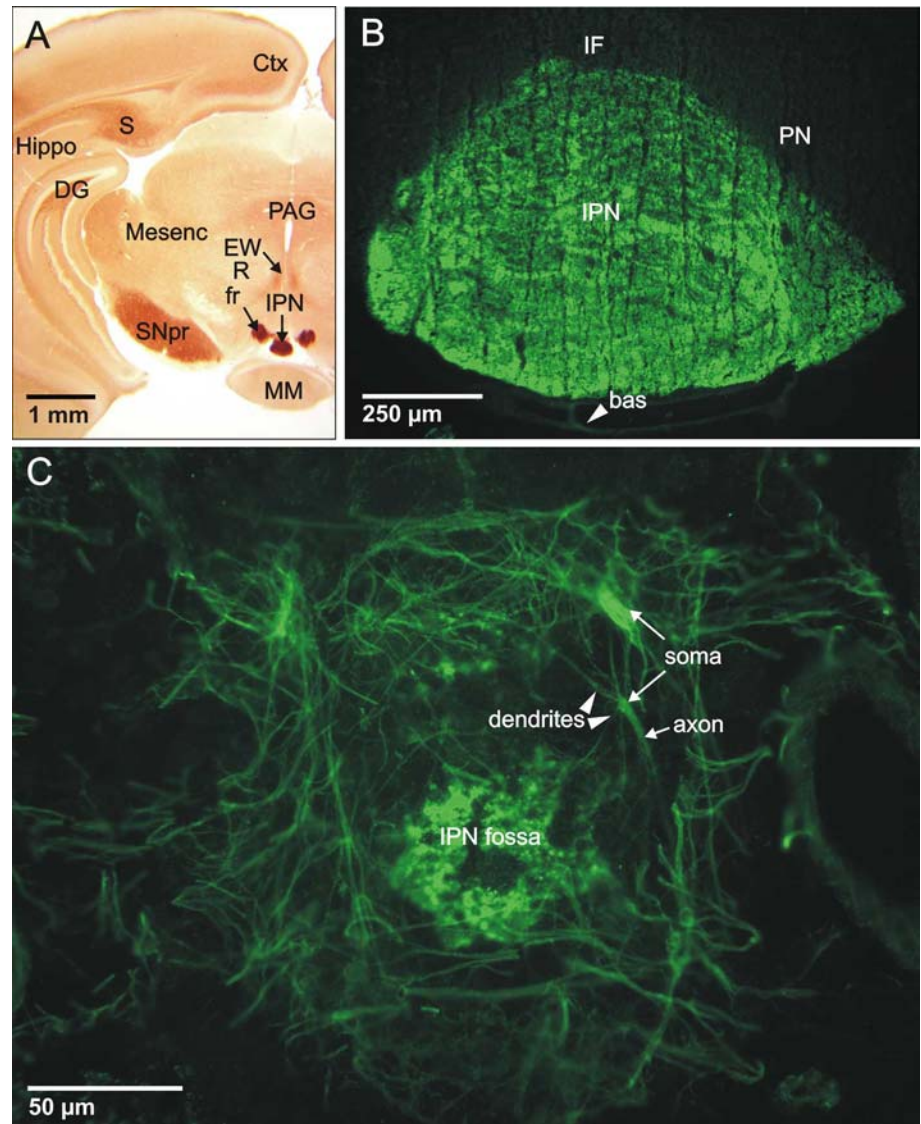
(Fig. 5a–c), dentate gyrus (Fig. 5a–d) and subiculum (Fig. 7a). In the hippocampal CA1, CA2 and CA3 region, BK channels are prominently expressed in the stratum oriens, which is composed of basket cells with ascending axons and ramifications of basal dendrites of the pyramidal cells, and the stratum lucidum, where mossy fibers from all parts of the granule cell layer of the dentate gyrus terminate at pyramidal neurons and interneurons (Fig. 5a, b). High levels of BK channel protein have also been detected in the stratum radiatum and the superficial part of the pyramidal cell layer (where CA3–CA1 associational fiber connections are located that are known as Schaffer collaterals). The stratum pyramidale itself shows only very low levels of immunoreactivity for BK channels (Fig. 5a, b). Under the medial border of the hippocampus and along the edge of its fissure, moderate (IF) to high (DAB) staining is observed in the molecular and polymorphic layer of the dentate gyrus (Fig. 5a, b), while the granule cells located in-between these layers display a faint

immunoreactivity (Fig. 5d). The subiculum as well as para- and presubiculum exhibit intense staining (Fig. 7b and Table 1).

#### Thalamus, habenula and hypothalamus

The thalamus constitutes the dorsal portion of the diencephalon and acts as a gatekeeper for information to the cerebral cortex. The thalamic nuclei are classified into the anterior-, medial-, lateral-, ventral- and posterior group. All of those nuclei display dense expression of BK channels (Fig. 6a, b, d). Above the thalamus, BK channels are highly concentrated in the medial habenular nucleus, a chief relay nucleus of the descending dorsal diencephalic conduction system (Fig. 6c, e). The habenulointerpeduncular tract (also termed fasciculus retroflexus) that emerges from the habenula proceeds to the medial edge of the red nucleus before terminating in the interpeduncular nucleus. Both, fasciculus retroflexus

**Fig. 7** Di- and mesencephalic BK channel expression sites. **a** Very high DAB stain is found in the fasciculus retroflexus (*fr*) and its projection area, the interpeduncular nucleus (*IPN*). High immunoreactivity is localized in cerebral cortex (*Ctx*), hippocampus (*Hippo*), dentate gyrus (*DG*), subiculum (*S*) and substantia nigra pars reticulata (*SNpr*). Moderate stain is found in the periaqueducal gray (*PAG*) and in the Edinger–Westphal nucleus (*EW*), whereas in the red nucleus (*R*) and in the mammillary nuclei (*MM*) the staining was low. **b** IF of interpeduncular nucleus (*IPN*) yields one of the highest signal in the mouse brain. The basilar artery (*bas*, arrowhead), interfascicular nucleus (*IF*) and paranigral nucleus (*PN*) is weakly stained. **c** Fossa of the interpeduncular nucleus (*IPN fossa*). Dendrites, somata, axons and terminals of neurons which project to and from the interpeduncular nucleus show IF, suggesting pre- and postsynaptic expression of BK channels



(Figs. 6c, e, 7a) and interpeduncular nucleus (the latter belonging to the mesencephalon) (Fig. 7a–c) express the highest levels of BK channel in the mouse brain. In contrast, very low density of the channel has been identified in hypothalamic areas (Fig. 3g) and associated nuclei (Fig. 6a, b).

### Mesencephalon

The mesencephalic nuclei and regions like red nucleus (Figs. 7a, 8a), raphe nuclei (Fig. 8a), Edinger–Westphal nucleus (Figs. 7a, 8a) and periaqueducal gray (Figs. 7a, 8a) express low to moderate levels of BK channels. The inferior colliculus shows moderate IF in the external and central cortex and a high IF in the dorsal cortex (Table 1). The lower immunoreactivity detected by DAB suggests that the fixation with paraformaldehyde may have masked antigenic structures of the BK channel in these neurons.

### Pons and medulla oblongata

Neurons in the pons receive and send information into the cerebellum or up to higher brain centers. The pontine nuclei (Fig. 8a, c, d), the pontine gray (Fig. 8b), the superior olivary complex as well as the tegmental nuclei express low levels of BK channels. Moderate immunoreactivity was found in Barrington nucleus, sphenoid nucleus and parabrachial nucleus (Table 1). The locus coeruleus providing noradrenergic input to forebrain, cerebellum, brainstem and spinal cord is remarkably stained (Fig. 8b). Significant expression is detected in all five vestibular nuclei (Fig. 9) that integrate signals from the vestibular organs with those from the spinal cord, cerebellum, and visual system and project to central targets. High immunoreactivity was observed in the vestibulocerebellar nucleus, the superior and the medial vestibular nucleus. Less intense staining was found in the lateral and the spinal vestibular nucleus, in the prepositus hypoglossal nucleus, the nuclei of the solitary tract,

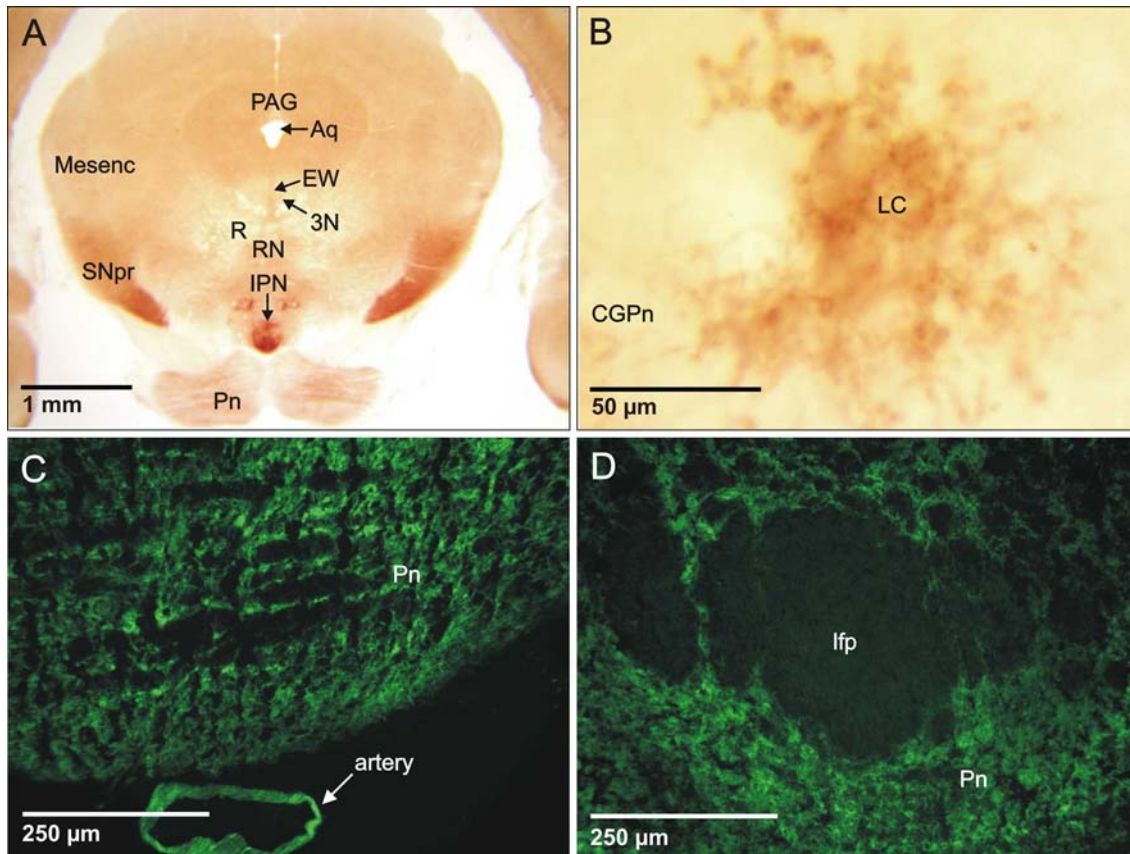


**Fig. 8** BK channel expression in midbrain and pons. **a** Low to moderate DAB stain in the periaqueducal gray (*PAG*), which surrounds the aqueduct of Sylvius (*Aq*), Edinger–Westphal nucleus (*EW*), oculomotor nucleus (*3N*), raphe nuclei (*RN*), red nucleus (*R*) and the pons with the pontine nuclei (*Pn*). For comparison, note the very prominent expression in the substantia nigra pars

reticulate (*SNpr*) and the interpeduncular nucleus (*IPN*). **b** The locus coeruleus (*LC*), the major noradrenergic nucleus in the brain and located near the central gray of the pons (*CGPn*), shows the highest DAB stain in the pons. **c** Note the IF stain of a brain artery. **d** No staining was observed in the longitudinal fasciculus of the pons (*lfp*)

the spinal trigeminal nucleus, the medullary raphe nuclei, the reticular nuclei and the dorsal motor nucleus of the vagus (Table 1). Low immunoreactivity was detected in the cochlear nuclei, the nuclei X and Y as well as in the cuneate nucleus and the gracile nucleus (Table 1).

### Cerebellum

Cerebellar regions receive projections from different portions of the brain and spinal cord and the output projections of the cerebellum are focused mainly on the premotor and motor systems. The cerebellum is composed of cerebellar cortex, internal white matter and three pairs of deep nuclei, the fastigial, the interposed, and the dentate. BK channels are mainly expressed in the cerebellar cortex, especially in the molecular layer (Fig. 10a–c). The molecular layer contains the cell bodies of two types of inhibitory interneurons, the stellate and basket cells, dispersed among the excitatory axons of granule cells and the dendrites of the inhibitory Purkinje cells. Further, the single layer of Purkinje cell

bodies with their axon hillocks is highly immunoreactive for BK channels (Fig. 10a, c, e). Positively stained axonal fibers and cell bodies are apparent in the innermost granular layer (Fig. 10b, d). The axonal structures may represent (a) Purkinje cell axons which project to the deep cerebellar nuclei and provide the only source of output from the cerebellar cortex, (b) mossy fibers originating from nuclei in the spinal cord and brain stem and/or (c) climbing fibers projecting from the inferior olivary nucleus. The weakly stained cell bodies in the granular layer may be granular cells and/or golgi cells (Fig. 10b, d). Beside the cerebellar cortex, BK channels are also abundantly present in all three deep cerebellar nuclei (Fig. 10b, e). These findings were consistent with the data from a previous study demonstrating BK channel  $\alpha$ -subunit expression in compartments of the cerebellar cortex and deep cerebellar nuclei (Sausbier et al. 2004). Additionally, immunofluorescence revealed a meshwork of stained axons in the white matter (Fig. 10d, e). These axons may represent Purkinje cell axons coursing through the white matter to terminate in deep cerebellar nuclei. The observed punctuated immu-

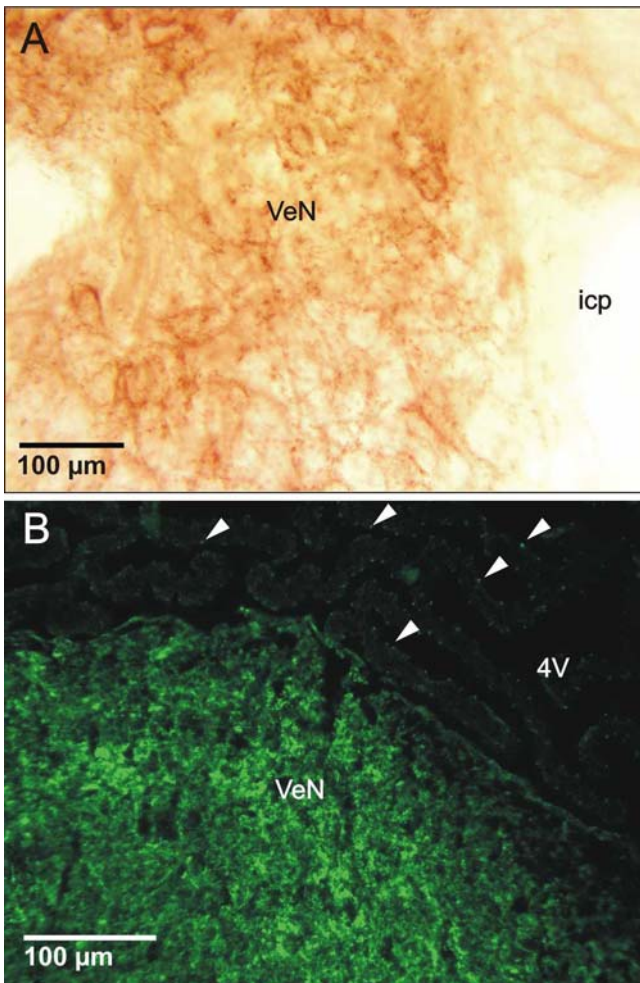


**Fig. 9** BK channel distribution in the medulla oblongata. **a** DAB staining reveals high expression in somata of vestibular nuclei (*VeN*) neurons and lack of expression in inferior cerebellar peduncle (*icp*). **b** IF also revealed expression in neurons of the vestibular nuclei (*VeN*). Punctuated IF (*arrowheads*) indicate blood vessels of choroid plexus of the fourth ventricle

nonfluorescence in these axons represents single or clustered BK channels (Fig. 10f).

## Discussion

The study presents a detailed BK channel  $\alpha$ -subunit distribution profile in the mouse brain and provides data regarding the subcellular localization of this channel to somato-dendritic/postsynaptic and axonal/presynaptic compartments. In this study, BK channel  $\alpha$ -subunit immunoreactivity was visualized by both DAB and IF and validated using the corresponding BK<sup>-/-</sup> brain sections as control. These two characteristics together with the fact that we analyzed the brain of a species used for genetic knockout models are the main differences compared to a previous study in rat (Knaus et al. 1996). Thus, behavioral studies, *in vitro* and *in vivo* findings

using knockout mouse models can directly be interpreted and understood. The findings of the present study clearly support previous electrophysiological data (Raffaelli et al. 2004; Hu et al. 2001; Isaacson and Murphy 2001). The outcome of these electrophysiological experiments was that diverse functions of BK channels, e.g., repolarization of action potentials, generating fast AHP (fAHP), contribute to the overall neuronal activity—depending on the investigated neuron. This functional variety could be due to the subcellular distribution of BK channels as demonstrated in this study. Furthermore, we found a high variability of BK channel expression within the diverse brain regions. The reason for that variability is not clear, but there may be a correlation between BK channel distribution and expression of voltage-gated Ca<sup>2+</sup> and Na<sup>+</sup> channels in these brain regions (see below).

In neurons, the main function of BK channels is the generation of the fAHP after a neuronal action potential. The large conductance of neuronal BK channels allows them to play an important role in hyperpolarizing the membrane potential when they are activated. Following the action potential and the fAHP, many neurons display a prolonged AHP lasting between hundreds of milliseconds and seconds. Depending on the neuronal subtypes, this AHP phase can be dissected into two main components: a medium (mAHP) and a slow AHP (sAHP) (Bond et al. 2004). It has been suggested that Ca<sup>2+</sup>-activated and voltage-independent K<sup>+</sup> channels of small conductance (SK channels) participate in the generation of mAHP and sAHP (Stocker et al. 1999; Gerlach et al. 2004). Hence, an overlap, at least in part, of BK and SK channel distribution would be expected. Comparison of the brain distribution of the SK channels (Sailer et al. 2004; Stocker and Pedarzani 2000) and the BK channel with respect to expression sites and densities revealed notable congruency of BK channels with SK3 channels in major parts of the tel-, di-, mes- and rhombencephalon. In contrast to the SK3 channel, considerable discrepancies were found between BK and SK1 channel expression, e.g., the low expression of SK1 in the di- and mesencephalon where BK channels are abundantly expressed. The SK2 channel also does not meet the expression density of BK channels in telencephalic regions like olfactory bulb and cerebral cortex, as well as in many parts of the di- and mesencephalon. The correlation between BK and SK3 channel expression densities in major brain regions suggests a functional relationship between both channels, conceivably in shaping AHP properties such as amplitude and duration, which in turn regulate interspike interval and spike-frequency adaptation of neuronal discharge activity (Ermentrout et al. 2001).

Apart from SK channels, the BK channel is also supposed to colocalize with voltage-gated Ca<sup>2+</sup> channels. The lack of BK channels reduces the spontaneous activity of the cerebellar Purkinje neurons (Sausbier et al. 2004) and possibly also of other neurons in the

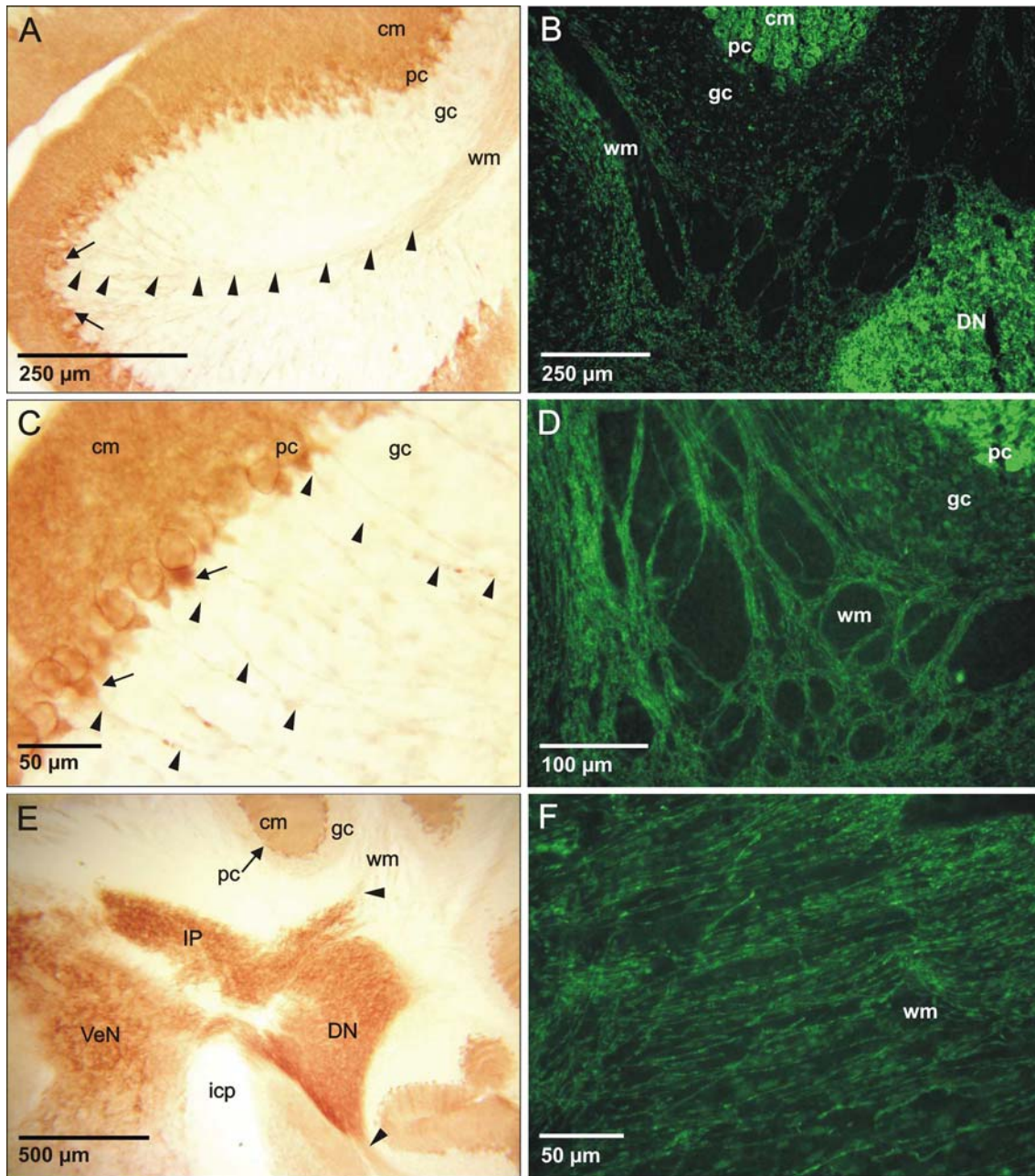


**Fig. 10** BK channels in the cerebellum. **a, c, e** Prominent DAB stain was detected both in the molecular layer (*cm*) containing the dendrites of Purkinje neurons, and in the Purkinje cell layer (*pc*), whereas the granule cell layer (*gc*) displayed only a weak signal. A detailed view on Purkinje neurons revealed a high intensity of BK channel staining in dendrites, axon hillock (*arrows*) and axons (*arrowheads*). (**E**) Purkinje axons project to deep cerebellar nuclei as the dentate nucleus (*DN*) and the nucleus interpositus (*IP*), both

displaying prominent immunoreactivity, as well as the vestibular nuclei (*VeN*). Immunostained axons project to/from the dentate nucleus (*DN*) and nucleus interpositus (*IP*) (*arrowheads*). **b, d** The meshwork of fluorescent axons in the white matter (*wm*) may represent Purkinje cell axons coursing through white matter to terminate in deep cerebellar nuclei. **f** Note the punctuated fluorescence labeling in axons representing single or clustered BK channels

CNS. This reduction in spontaneous discharge is caused by the lack of postsynaptic BK channels and has been found to be due to depolarization-induced inactivation of the action potential mechanism. These previous findings suggested that the reset of voltage-gated  $\text{Ca}^{2+}$  and  $\text{Na}^{+}$  channels from inactivation was impaired when neurons chronically lack BK channels

and therewith the fAHP component and the BK channel's influence on resting membrane potential. Indeed,  $\text{Ca}^{2+}$  entry through voltage-gated calcium channels can activate either large-(BK) or small-(SK) conductance calcium-activated potassium channels. A putative functional coupling between BK channels and neuronal voltage-gated  $\text{Ca}^{2+}$  channels of the  $\text{Ca}_v1.2$

and  $\text{Ca}_v1.3$  L-type is reflected by their grossly overlapping distribution pattern with the BK channel expression profile (Grunnet and Kaufmann 2004). However, the relationship between  $\text{Ca}^{2+}$  currents and  $\text{Ca}^{2+}$ -activated  $\text{K}^+$  currents depends on the subcellular localization of these channels and on intracellular  $\text{Ca}^{2+}$  accumulation during neural activity and may vary from neuron type to neuron type. For example, in hippocampal neurons L-type channels only activate SK channels, whereas N-type  $\text{Ca}^{2+}$  channels selectively activate BK channels (Marrion and Tavalin 1998). Unlike hippocampal neurons, both the L- and N-type  $\text{Ca}^{2+}$  channels induce BK currents in neocortical pyramidal neurons (Sun et al. 2003). Further, P/Q- and T-type  $\text{Ca}^{2+}$  channels control the activity of BK channels in Purkinje (Edgerton and Reinhart 2003) and vestibular nucleus neurons (Smith et al. 2002), respectively. Taken together, the expression profile of BK channels presented in this study likely points to a functional coupling with voltage-gated  $\text{Ca}^{2+}$  and  $\text{Na}^+$  channels in the CNS.

What can we learn from the BK channel mapping in regard to neurological disorders and their characterization using knockout mouse models? In the last few years, the understanding of how ion channels function at the molecular and cellular level and how channel gene mutations can cause neurological symptoms deepened (Cooper and Jan 1999). There are increasing implications that gain-of-function and loss-of-function mutations of potassium channels are the cause of neurological disorders, such as epilepsy, cerebellar ataxia and paroxysmal movement disorders (Eunson et al. 2000; Rogawski 2000; Watanabe et al. 2000; Du et al. 2005; Sausbier et al. 2004; Turnbull et al. 2005). In epilepsy, a sudden synchronous discharge of neurons throughout the brain causes primarily generalized seizures based on a genetically determined generalized hyperexcitability of neurons (Turnbull et al. 2005). Interestingly, the neuronal nicotinic acetylcholine receptor  $\alpha 4$  subunit encoded by *CHRNA4*, the first discovered epilepsy gene (Steinlein et al. 1995), displays an expression profile throughout the whole brain. Thus, at least in the case of *CHRNA4*, the observed generalized hyperexcitability due to mutations in this gene could be correlated with the widely expression of the corresponding protein throughout the brain. However, this correlation seems to work also in the case of *KCNMA1*, the gene encoding the pore-forming  $\alpha$ -subunit of BK channels, because a recent study demonstrated that a mutation of the widely expressed BK channel  $\alpha$ -subunit causes generalized epilepsy in human (Du et al. 2005). In turn, the findings of our study, e.g., widely expression of BK channels in pre- and postsynaptic compartments, will help to understand why a gain-of-function mutation in BK channel  $\alpha$ -subunits cause a generalized epilepsy. A gain-of-function mutation of BK channels could also be induced by targeted deletion of the neuron-specific inhibitory  $\beta 4$  subunit of the BK channel in mice. BK  $\beta 4$  subunit knockout mice should exhibit a hyperexcitability of neurons due to

an increased activity of BK channels which is associated with epilepsy (Du et al. 2005).

An interesting and increasingly recognized phenomenon is the coexistence of epilepsy and paroxysmal dyskinesia in the same individual (Guerrini 2001; Guerrini et al. 2002). Despite the fact that the basic pathophysiology underlying that coexistence is unknown, both neurological disorders seems to be the clinical consequence from a gain-of-function mutation of BK channels leading to an increase in neuronal excitability (Du et al. 2005). In paroxysmal dyskinesia, the dysfunction of the basal ganglia was—at least in part—due to a gain-of-function mutation of the BK channel in affected individuals. This observation is supported by our mapping study demonstrating high expression levels of BK channel in basal ganglia. The dyskinesia in these individuals was triggered in a synergistic manner by alcohol and the gain-of-function mutation of BK channel. It has been shown that ethanol at relevant clinical concentrations increases the activity of BK channels in various neurons/compartments including cerebellar Purkinje cells (Carlen et al. 1984), dentate granule cells from hippocampus (Niesen et al. 1988) as well as CA1 and CA3 hippocampal neurons (Carlen et al. 1982). The electrophysiological identification of BK channel currents in these investigated neurons/compartments is consistent with the BK channel protein expression presented in this study. However, the BK channel distribution profile in brain points to a generalized effect of ethanol in the CNS. In fact, genetic studies demonstrated that only the BK channel  $\alpha$ -subunit expressed in the nervous system mediates ethanol sensitivity (Davies et al. 2003). Analyzing the knockout mouse will help to clarify the relationship between BK channel distribution in brain, biochemical effect of ethanol in vivo, and behavioral effects in mammalian. In conclusion, our BK channel  $\alpha$ -subunit mapping will be a helpful tool for interpretation and understanding in vitro and in vivo findings and will facilitate functional characterization of genetically manipulated mice.

**Acknowledgements** We thank Isolde Breuning and Clement Kabbage for excellent technical assistance, Johan Storm for critical reading the manuscript and Deutsche Forschungsgemeinschaft for financial support.

## References

- Bond CT, Herson PS, Strassmaier T, Hammond R, Stackman R, Maylie J, Adelman JP (2004) Small conductance  $\text{Ca}^{2+}$ -activated  $\text{K}^+$  channel knock-out mice reveal the identity of calcium-dependent afterhyperpolarization currents. *J Neurosci* 24:5301–5306
- Butler A, Tsunoda S, McCobb DP, Wei A, Salkoff L (1993) mSlo, a complex mouse gene encoding “maxi” calcium-activated potassium channels. *Science* 261:221–224
- Carlen PL, Gurevich N, Durand D (1982) Ethanol in low doses augments calcium-mediated mechanisms measured intracellularly in hippocampal neurons. *Science* 215:306–309

- Carlen PL, Wilkinson DA, Wortzman G, Holgate R (1984) Partially reversible cerebral atrophy and functional improvement in recently abstinent alcoholics. *Can J Neurol Sci* 11(4):441–446
- Chavis P, Ango F, Michel JM, Bockaert J, Fagni L (1998) Modulation of big  $K^+$  channel activity by ryanodine receptors and L-type  $Ca^{2+}$  channels in neurons. *Eur J Neurosci* 10:2322–2327
- Cooper EC, Jan LY (1999) Ion channel genes and human neurological disease: recent progress, prospects, and challenges. *Proc Natl Acad Sci USA* 96:4759–4766
- Davies AG, Pierce-Shimomura JT, Kim H, VanHoven MK, Thiele TR, Bonci A, Bargmann CI, McIntire SL (2003) A central role of the BK potassium channel in behavioral responses to ethanol in *C. elegans*. *Cell* 115:655–666
- Du W, Bautista JF, Yang H, Diez-Sampedro A, You SA, Wang L, Kotagal P, Lüders HO, Shi J, Cui J, Richerson GB, Wang QK (2005) Calcium-sensitive potassium channelopathy in human epilepsy and paroxysmal movement disorder. *Nat Genet* 37:733–738
- Edgerton JR, Reinhart PH (2003) Distinct contributions of small and large conductance  $Ca^{2+}$ -activated  $K^+$  channels to rat Purkinje neuron function. *J Physiol* 548:53–69
- Ermentrout B, Pascal M, Gutkin B (2001) The effects of spike frequency adaptation and negative feedback on the synchronization of neural oscillators. *Neural Comput* 13:1285–1310
- Eunson LH, Rea R, Zuberi SM, Youroukos S, Panayiotopoulos CP, Liguori R, Avoni P, McWilliam RC, Stepenson JB, Hanna MG, Kullmann DM, Spauschus A (2000) Clinical, genetic, and expression studies of mutations in the potassium channel gene *KCNA1* reveal new phenotypic variability. *Ann Neurol* 48:647–656
- Faber ES, Sah P (2003) Calcium-activated potassium channels: multiple contributions to neuronal function. *Neuroscientist* 9:181–194
- Gerlach AC, Maylie J, Adelman JP (2004) Activation kinetics of the slow afterhyperpolarization in hippocampal CA1 neurons. *Pflugers Arch* 448:187–196
- Grunnet M, Kaufmann WA (2004) Coassembly of big conductance  $Ca^{2+}$ -activated  $K^+$  channels and L-type voltage-gated  $Ca^{2+}$  channels in rat brain. *J Biol Chem* 279:36445–36453
- Guerrini R (2001) Idiopathic epilepsy and paroxysmal dyskinesia. *Epilepsia* 42:36–41
- Guerrini R, Sanchez-Carpintero R, Deonna T, Santucci M, Bhatia KP, Moreno T, Parmeggiani L, Bernardina BD (2002) Early-onset absence epilepsy and paroxysmal dyskinesia. *Epilepsia* 43:1224–1229
- Hu H, Shao LR, Chavoshy S, Gu N, Trieb M, Behrens R, Laake P, Pongs O, Knaus HG, Ottersen OP, Storm JF (2001) Presynaptic  $Ca^{2+}$ -activated  $K^+$  channels in glutamatergic hippocampal terminals and their role in spike repolarization and regulation of transmitter release. *J Neurosci* 21:9585–9597
- Hirst WD, Abrahamsen B, Blaney FE, Calver AR, Aloj L, Price GW, Medhurst AD (2003) Differences in the central nervous system distribution and pharmacology of the mouse 5-hydroxytryptamine-6 receptor compared with rat and human receptors investigated by radioligand binding, site-directed mutagenesis, and molecular modeling. *Mol Pharmacol* 64:1295–1308
- Isaacson JS, Murphy GJ (2001) Glutamate-mediated extrasynaptic inhibition: direct coupling of NMDA receptors to  $Ca^{2+}$ -activated  $K^+$  channels. *Neuron* 31:1027–1034
- Jan LY, Jan YN (1997) Ways and means for left shifts in the MaxiK channel. *Proc Natl Acad Sci USA* 94:13383–13385
- Knaus HG, Schwarzer C, Koch RO, Eberhart A, Kaczorowski GJ, Glossmann H, Wunder F, Pongs O, Garcia ML, Sperk G (1996) Distribution of high-conductance  $Ca^{2+}$ -activated  $K^+$  channels in rat brain: targeting to axons and nerve terminals. *J Neurosci* 16:955–963
- Larm JA, Shen PJ, Gundlach AL (2003) Differential galanin receptor-1 and galanin expression by 5-HT neurons in dorsal raphe nucleus of rat and mouse: evidence for species-dependent modulation of serotonin transmission. *Eur J Neurosci* 17:481–493
- Levitan IB, Adams WB (1981) Cyclic AMP modulation of a specific ion channel in an identified nerve cell: possible role for protein phosphorylation. *Adv Cyclic Nucleotide Res* 14:647–653
- Marrion NV, Tavalin SJ (1998) Selective activation of  $Ca^{2+}$ -activated  $K^+$  channels by co-localized  $Ca^{2+}$  channels in hippocampal neurons. *Nature* 395:900–905
- Niesen CE, Baskys A, Carlen PL (1988) Reversed ethanol effects on potassium conductances in aged hippocampal dentate granule neurons. *Brain Res* 445:137–141
- Paxinos G, Franklin KBJ (2004) *The mouse brain in stereotaxic coordinates*, 2nd edn. Academic, San Diego
- Piggins HD, Samuels RE, Coogan AN, Cutler DJ (2001) Distribution of substance P and neurokinin-1 receptor immunoreactivity in the suprachiasmatic nuclei and intergeniculate leaflet of hamster, mouse, and rat. *J Comp Neurol* 438:50–65
- Raffaelli G, Saviane C, Mohajerani MH, Pedarzani P, Cherubini E (2004) BK potassium channels control transmitter release at CA3–CA3 synapses in the rat hippocampus. *J Physiol* 557:147–157
- Robitaille R, Thomas S, Charlton MP (1999) Effects of adenosine on  $Ca^{2+}$  entry in the nerve terminal of the frog neuromuscular junction. *Can J Physiol Pharmacol* 77:707–714
- Rogawski MA (2000) *KCNQ2/KCNQ3*  $K^+$  channels and the molecular pathogenesis of epilepsy: implications for therapy. *Trends Neurosci* 23:393–398
- Sailer CA, Kaufmann WA, Marksteiner J, Knaus HG (2004) Comparative immunohistochemical distribution of three small-conductance  $Ca^{2+}$ -activated potassium channel subunits, SK1, SK2, and SK3 in mouse brain. *Mol Cell Neurosci* 26:458–469
- Sausbier M, Hu H, Arntz C, Feil S, Kamm S, Adelsberger H, Sausbier U, Sailer CA, Feil R, Hofmann F, Korth M, Shipston MJ, Knaus HG, Wolfer DP, Pedroarena CM, Storm JF, Ruth P (2004) Cerebellar ataxia and Purkinje cell dysfunction caused by  $Ca^{2+}$ -activated  $K^+$  channel deficiency. *Proc Natl Acad Sci USA* 101:9474–9478
- Shao LR, Halvorsrud R, Borg-Graham L, Storm JF (1999) The role of BK-type  $Ca^{2+}$ -dependent  $K^+$  channels in spike broadening during repetitive firing in rat hippocampal pyramidal cells. *J Physiol* 521:135–146
- Shipston MJ (2001) Alternative splicing of potassium channels: a dynamic switch of cellular excitability. *Trends Cell Biol* 11:353–358
- Smith MR, Nelson AB, Du Lac S (2002) Regulation of firing response gain by calcium-dependent mechanisms in vestibular nucleus neurons. *J Neurophysiol* 87:2031–2042
- Steinlein OK, Mulley JC, Propping P, Wallace RH, Phillips HA, Sutherland GR, Scheffer IE, Berkovic SF (1995) A missense mutation in the neuronal nicotinic acetylcholine receptor alpha 4 subunit is associated with autosomal dominant nocturnal frontal lobe epilepsy. *Nat Genet* 11:201–203
- Stocker M, Krause M, Pedarzani P (1999) An apamin-sensitive  $Ca^{2+}$ -activated  $K^+$  current in hippocampal pyramidal neurons. *Proc Natl Acad Sci USA* 96:4662–4667
- Stocker M, Pedarzani P (2000) Differential distribution of three  $Ca^{2+}$ -activated  $K^+$  channel subunits, SK1, SK2, and SK3, in the adult rat central nervous system. *Mol Cell Neurosci* 15:476–493
- Storm JF (1987) Action potential repolarization and a fast after-hyperpolarization in rat hippocampal pyramidal cells. *J Physiol* 385:733–759
- Storm JF (1990) Potassium currents in hippocampal pyramidal cells. *Prog Brain Res* 83:161–187
- Sun X, Gu XQ, Haddad GG (2003) Calcium influx via L- and N-type calcium channels activates a transient large-conductance  $Ca^{2+}$ -activated  $K^+$  current in mouse neocortical pyramidal neurons. *J Neurosci* 23:3639–3648
- Turnbull J, Lohi H, Kearney JA, Rouleau GA, Delgado-Escueta AV, Meisler MH, Cossette P, Minassian BA (2005) Sacred disease secrets revealed: the genetics of human epilepsy. *Hum Mol Genet* 14:2491–2500



- Watanabe H, Nagata E, Kosakai A, Nakamura M, Yokoyama M, Tanaka K, Sasai H (2000) Disruption of the epilepsy KCNQ2 gene results in neural hyperexcitability. *J Neurochem* 75:28–33
- Womack MD, Khodakhah K (2004) Dendritic control of spontaneous bursting in cerebellar Purkinje cells. *J Neurosci* 24:3511–3521
- Womack MD, Chevez C, Khodakhah K (2004) Calcium-activated potassium channels are selectively coupled to P/Q-type calcium channels in cerebellar Purkinje neurons. *J Neurosci* 24:8818–8822